CERN – EUROPEAN ORGANIZATION FOR NUCLEAR RESEARCH

CLIC – Note – 1198

# DESIGN, FABRICATION AND RF MEASUREMENTS OF THE STORAGE AND CORRECTION CAVITY PROTOTYPES OF THE RF PULSE COMPRESSION SYSTEM FOR THE KLYSTRON-BASED CLIC MAIN LINAC

P. Wang and A. Grudiev, B. Riffaud, E. Berthome, F. Motschmann, I. Syratchev, K. Scibor, L. Giordanino, N. Catalan Lasheras and P. Morales Sanchez

CERN, Geneva, Switzerland

CERN-ACC-2024-0003
09/10/2024

**Abstract**

An RF pulse compression system based on double-height waveguides was studied for the Klystron-based CLIC main linac. The optimized power gain of the new system is 3.78, with a specific output pulse shape required for the transient beamloading compensation. A method based on the waveform parameters of the input pulse was introduced to achieve such an output pulse shape. This pulse compression system consists of a storage cavity of a Barrel Open Cavity (BOC) type and four correction cavities. The BOC storage cavity has a Q0 of 2.35 × 105 with the TM32,1,1 mode and a β of 6.6. A novel RF coupler was designed to facilitate the machining procedure of the BOC storage cavity. For the correction cavities, a bowl cavity with the TE1,2,4 mode and a spherical cavity with the TE1,1,3 mode were selected for the potential correction chain. Three prototypes were designed, fabricated, and RF measured validating the fabrication procedure for the series production.

Geneva, Switzerland
October 2024

# Design, fabrication and RF measurements of the storage and correction cavity prototypes of the RF pulse compression system for the klystron-based CLIC main linac

Ping Wang,* Alexej Grudiev, Benoit Riffaud, Emmanuel Berthome, Fritz Motschmann, Igor Syratchev, Karol Scibor, Laurene Giordanino, Nuria Catalan Lasheras, and Pedro Morales Scanchez
*CERN, CH-1211 Geneva-23, Swtizerland*
(Dated: August 27, 2024)

An RF pulse compression system based on double-height waveguides was studied for the Klystron-based CLIC main linac. The optimized power gain of the new system is 3.78, with a specific output pulse shape required for the transient beamloading compensation. A method based on the waveform parameters of the input pulse was introduced to achieve such an output pulse shape. This pulse compression system consists of a storage cavity of a Barrel Open Cavity (BOC) type and four correction cavities. The BOC storage cavity has a $Q_0$ of $2.35 \times 10^5$ with the $TM_{32,1,1}$ mode and a $\beta$ of 6.6. A novel RF coupler was designed to facilitate the machining procedure of the BOC storage cavity. For the correction cavities, a bowl cavity with the $TE_{1,2,4}$ mode and a spherical cavity with the $TE_{1,1,3}$ mode were selected for the potential correction chain. Three prototypes were designed, fabricated, and RF measured validating the fabrication procedure for the series production.

## I. INTRODUCTION

The klystron-based Compact Linear Collider (CLIC), with the center-of-mass collision energy of 380 GeV, utilizes klystrons as RF sources for the main beam acceleration [1, 2]. To reduce the number of klystrons and the overall cost of the RF system, an RF pulse compression system is employed, as in many other projects [3–7]. The pulse compression system compresses long input RF pulses and generates shorter RF pulses with a much larger peak power. The power gain, defined as the peak output power over the peak input power, is strongly related to the unloaded quality of the resonant cavities of the RF pulse compression system and the length of the compressed output pulse. In general, the power gain is higher for large unloaded quality factors and short output pulse lengths. However, the length of the compressed RF pulses going into the linacs should be as long as possible for efficient multi-bunch acceleration to achieve the high-luminosity in CLIC. In addition, these RF pulses should have a specific shape to compensate for the transient beam loading effect, the details can be seen in [8, 9].

To meet the requirements of high power gain, long output pulse and specific pulse shape, an RF pulse compression system based on individual cavities was studied in 1992[10]. These individual cavities are defined as the storage cavity (SC) and the correction cavity (CC). Only the SC requires a large unloaded quality factor, which determines the efficiency and power gain of the pulse compression system. Several CCs are used to modulate the amplitude of the input RF pulses. Each cavity of the pulse compression system produces an RF peak in the spectrum, similar to that of the SLED-II pulse compressor[11], which uses long delay lines and generates flat output RF pulses.

A pulse compression system based on a correction cavity chain and an SLEDX pulse compressor was designed and fabricated to demonstrate the technique based on the SC and CCs[12]. The correction cavity chain consists of eight spherical cavities with an unloaded quality factor of about $4.5 \times 10^4$ and four H-Rotators. The correction cavity chain was manufactured and tested in the Xbox-2 high-power test at CERN[13]. The test results showed that the correction cavities efficiently modulate the amplitude of the RF pulse. This type of correction cavity chain was also applied for an X-band two-stage pulse compressor in the X-band high-power test at Tsinghua University[14]. The SC, which is an SLEDX pulse compressor, has an unloaded quality factor of $1.77 \times 10^5$. This SC, together with the CC chain, generates RF pulses with a flat top of 244 ns and a power gain of 3.54, resulting in high peak power from the klystrons[15]. To reduce the requirement for the klystron peak RF power, the unloaded quality factors of the SC and CCs are recommended as $2.4 \times 10^5$ and $6.0 \times 10^4$, respectively[15].

Among the existing X-band pulse compressors, the BOC pulse compressor from PSI has a maximum unloaded quality factor of $1.5 \times 10^5$, which is still far from $2.4 \times 10^5$[13, 16]. A novel large bowl cavity was designed with an unloaded quality factor of $2.42 \times 10^5$[17]. The fabrication of the prototype for the large bowl cavity is currently underway. For the CCs, an X-band spherical pulse compressor with an unloaded quality of $9.6 \times 10^4$ and an X-band corrugated pulse compressor with an unloaded quality of $1.4 \times 10^5$ are good candidates[18, 19]. They have been tested at high power and showed good high-power performances. These X-band pulse compressors use an H-Rotator and a single resonant cavity, which benefits the compactness of the correction cavity chain. A small bowl cavity was also designed for the correction cavity chain[17]. In addition, another two cylinder cavity based cavity types were designed for the correction cavity chain. However, prototypes are needed to verify their

* ping.wang@cern.ch

reliability and feasibility[20].

An improvement to the klystron-based CLIC is the application of the double height waveguide (DHW). Using a waveguide with a height of 20.32 mm, the surface fields and the RF loss of the waveguide can be reduced by 30% and 40%, respectively. This dramatically improves the high power performance of the waveguide network[21]. Based on the new requirements of the RF pulse compression system and the application of the DHW, the RF system requires updates. In this paper, we focus mainly on the RF pulse compression system. For the SC, we proposed a BOC storage cavity with a novel RF power coupler and the DHW. For the CCs, we proposed a bowl correction cavity with the $TE_{124}$ mode and a spherical correction cavity with the $TE_{113}$ mode. Both candidates deploy an H-Rotator for RF power coupling from the rectangular waveguide to the rotating circular waveguide mode as an input in the CC.

The structure of this paper is as follows. Sect.II. will discuss the waveform calculations which take into account the specific pulse shape required by the CLIC-K linac[8, 9]. The details of the BOC storage cavity will be presented in the Sect.III including the RF design, the mechanical design, the thermal analysis as well as the fabrication and the results of the RF measurements. In Sect.IV, we describe the RF designs, the mechanical designs, and the results of the RF measurements of the bowl and spherical cavities. Finally, we formulate a conclusion in Sect.V.

## II. WAVEFORM CALCULATIONS

An accelerating structure named CLIC-K was designed for the klystron-based CLIC [9]. To compensate for the transient beamloading effect, a specific shape of the input pulse is needed. In the case of CLIC-K, four parameters define this requirement: the filling time of the structure ($\tau_f$), the beam time ($\tau_b$), the power at the beginning of the filling time ($P_f$), and the peak input power ($P_{in}$), as shown in Fig. 1. The values of the parameters are listed in Table I. The pulse compression system should generate RF pulses that meet the shape requirement for the beamloading compensation. For more details about the beamloading compensation, please refer to [9].

TABLE I. Parameters of the pulse shape for the CLIC-K

| Parameters | Symbol | Unit | Value |
|---|---|---|---|
| Filling time | $\tau_f$ | $ns$ | 63.6 |
| Beam time | $\tau_b$ | $ns$ | 242 |
| Filling input power | $P_f$ | $MW$ | 10.15 |
| Peak input power | $P_{in}$ | $MW$ | 40.6 |

Figure 2 shows the normalized input and output waveforms, as well as the input and output phases of the pulse compression system. The outputs can be calculated based on the spectrum of the pulse compression

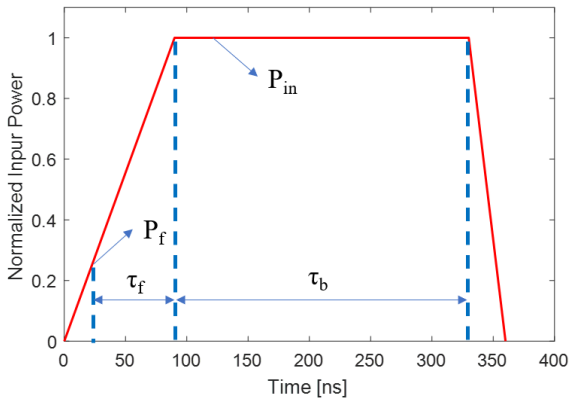


FIG. 1. Parameters of the input waveform for the beamloading compensation of the CLIC-K structure.

system and the input pulses. For more details, please see [12]. The original input pulse (the blue dashed curve) is flat. The pulse compression system compresses this input pulse and generates the output pulse with several ripples. To get a flat-top output pulse, the amplitude modulation is applied to the input pulse. The $Ptau$ is the normalized power at the beginning of the filling time and $Pg$ is the average normalized power of the flat top of the output pulse which is the same as the power gain of the pulse compression system. The ratio of $Ptau$ over $Pg$ should be the same as the ratio of $P_f$ over $P_{in}$ as mentioned above. The $PinMax$ and $PoutMax$ are the maximum points of the input waveform and output waveform. During the modulation, $PinMax$ should be 1 and $PinMax$ should equals to $Pg$.

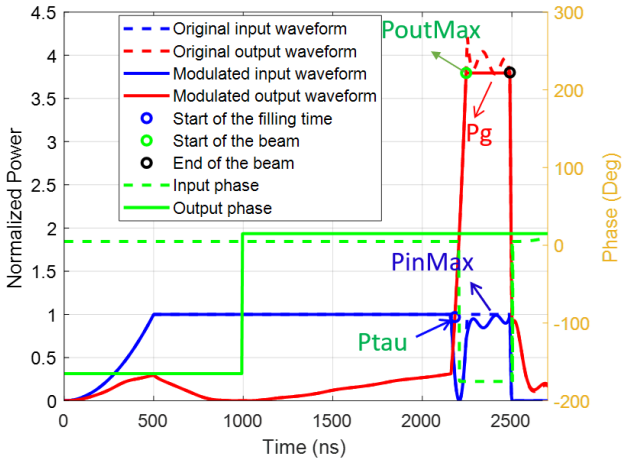


FIG. 2. Input and output waveforms as well as the input and output phases of the pulse compression system

The output pulse was optimized using the parameters $td$, $rt$, and $D$, as shown in Fig. 3. $D$ is used to limit the length of the flat top and $td$ is used to define the start point of the beam time. The $rt$ is the key parameter to optimize the shape of the output pulse. It determines

the slope of the leading edge of the output pulse and simultaneously greatly affects the amplitudes of the ripples of the output pulse before the modulation. As shown in Fig. 4, the amplitudes of the ripples are dramatically reduced by using a larger $rt$.

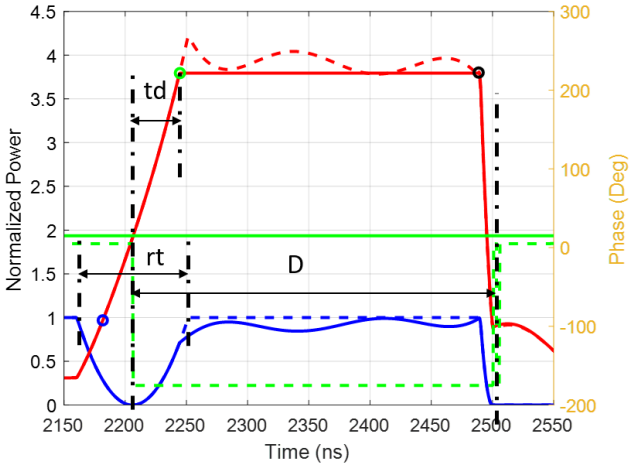


FIG. 3. Zoom in of Fig. 2 with a range of from 2100 ns to 2550 ns

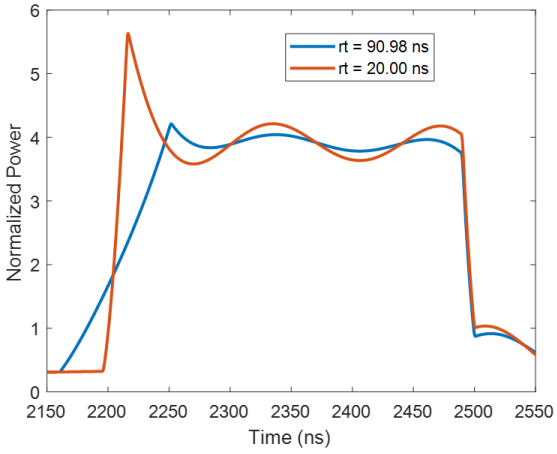


FIG. 4. Output waveforms with different $rt$ parameters

A merit function is defined based on the parameters of the input and output waveforms mentioned above:

$$MeritFun(td, rt, D, \beta_c) = |PinMax - 1| + |PoutMax/Pg - 1| + |Ptau/Pg - P_f/P_{in}| \quad (1)$$

where $\beta_c$ is the coupling factor of the correction cavities. All unloaded quality factors of the SC and CCs are from the RF designs, which are fixed in the waveform optimization. In this section, the unloaded quality factors are $2.35 \times 10^5$ for the SC and $7.5 \times 10^4$ for CCs. They will be discussed in Sect.III and Sect.IV. Another fixed parameter in the waveform optimization is $\beta_s$, which is the coupling factor of the SC. For different $\beta_s$, an output pulse with the required shape can be obtained by minimizing $MeritFun(td, rt, D, \beta_c)$. The power gain curve versus $\beta_s$, which provides the optimized $\beta_s$ is shown in Fig. 5. The optimal coupling factor of the SC is 6.2. However, in case of the reduction of unloaded quality factor of the SC, a larger coupling factor is preferable. A coupling factor of 6.6 was chosen, as the power gain is only 0.5% lower than the optimized value. At this point, the optimization of the pulse compression system is complete. This optimization procedure takes into account the shape of the output pulse. The power gain also benefits from this optimization procedure, which takes advantage of the $rt$ parameter to reduce the amplitudes of the ripples. The final parameters for the input waveform after the optimization are shown in Table II.

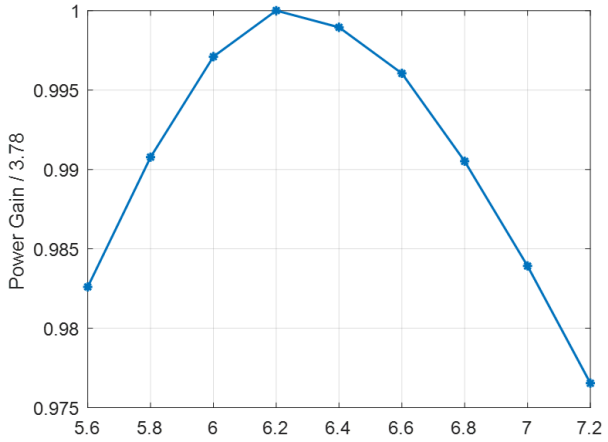


FIG. 5. Power gain versus the coupling factor of the SC

TABLE II. Main parameters of the input pulse

| Parameters and units | Value |
|---|---|
| Input pulse length [ns] | 2500 |
| $rt$ [ns] | 90.98 |
| $td$ [ns] | 38.69 |
| $D$ [ns] | 290.69 |

In principle, the more the CCs are in the RF pulse compression system, the larger is the power gain. However, the more CCs, the more the RF losses are introduced by the CCs which reduces the power gain. In addition, the slope of the leading edge of the output pulse is also useful to reduce the ripple amplitude. Taking these factors into account, the number of CCs must be optimized. Figure 6 shows the power gains versus the number of CCs for three cases. In the first case, no RF loss is included. For the other two cases, the H-Rotator is assumed for the correction cavities and used for one CC or for two CCs. For all the three cases, the optimized number of the CCs is 4. The RF parameters of five resonant cavities in the RF pulse compression system are shown in Table III. The

corresponding power gain without RF loss is 3.78. An RF module for the klystron-based CLIC consists of two klystrons with an output power of 50 MW each, an RF pulse compression system and eight CLIC-K structures with an input power of 40.6 MW[21]. The relationship of the output power of the klystron($P_k$), the input power of the CLIC-K ($P_{in}$), the power gain of the pulse compression system ($Pg$) and the RF loss of the RF system ($\eta$) is that $P_k * 2 * Pg * (1-\eta) \geq 8 * P_{in}$. The $\eta$ of the RF system is 10.66% or 12.25 % for two different methods to meet the Beam Based Alignment requirements[21]. The minimum required $Pg$ is 3.64 or 3.70 for the two cases. Both are smaller than 3.78 of the proposed design meeting the requirements. The $S_{12}$ of the RF pulse compression system shown in Fig. 7.

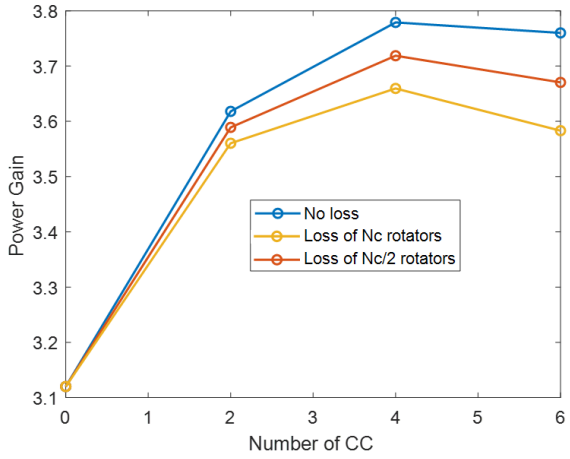


FIG. 6. Power gain versus the number of CCs.

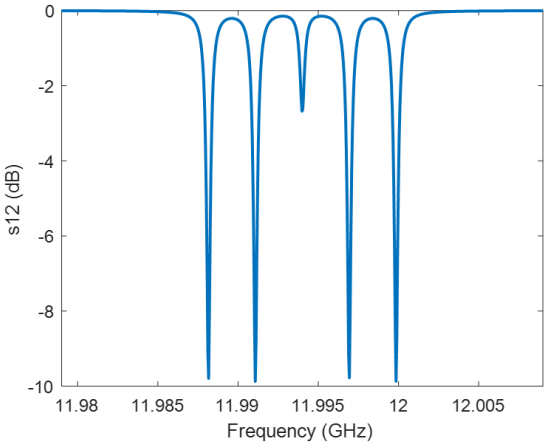


FIG. 7. $S_{12}$ of the pulse compression system.

TABLE III. RF parameters of the pulse compression system

| | Frequency [GHz] | $Q_0$ | $Q_e$ | $\beta$ |
|---|---|---|---|---|
| CC1 | 11.9882 | 7.5e4 | 3.85e4 | 1.95 |
| CC2 | 11.9911 | 7.5e4 | 3.85e4 | 1.95 |
| SC | 11.9940 | 23.5e4 | 3.56e4 | 6.6 |
| CC3 | 11.9969 | 7.5e4 | 3.85e4 | 1.95 |
| CC4 | 11.9998 | 7.5e4 | 3.85e4 | 1.95 |

## III. BOC STORAGE CAVITY

In this section, the RF design, mechanical design, thermal analysis, fabrication and RF measurement results of the BOC prototype are presented. BOC pulse compressors have advantages of large unloaded quality factor, lower surface fields and large mode seperations. They were studied and successfully implemented in CLIC Test Facility (S-band), Swiss FEL (C- and X-band) and DESY (X-band)[16, 22–24]. As the SC of the RF pulse compression system needs a large unloaded quality factor as large as about $2.4 \times 10^5$, the BOC storage cavity is the best option.

### A. RF design of the BOC storage cavity

The RF model and the field pattern are shown in Fig. 8 and Fig. 9. It consists of a barrel open cavity, a DHW around the cavity, and a novel RF coupler. The working mode of the cavity is $TM_{32,1,1}$. In the spherical coordinate system, 32 is the mode index in the azimuthal direction. Traditional BOC pulse compressors need fake coupling holes to keep the symmetry of the cavity and optimize the reflection. However, a feature of this BOC storage cavity is that no fake coupling holes are used for keeping the cavity symmetry, which benefits from the application of the novel RF coupler.

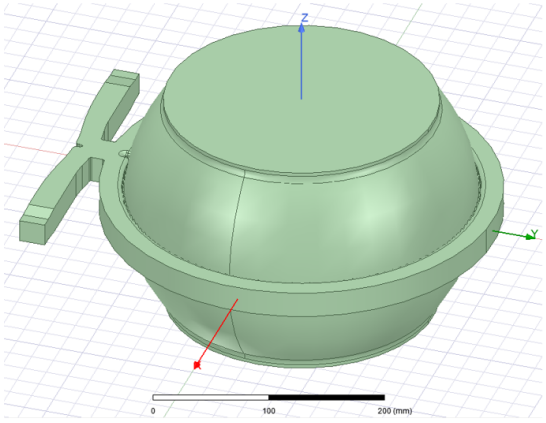


FIG. 8. Full RF model of the BOC storage cavity.

The shape of the cavity is described by five parameters as shown in Fig 10. The two main parameters are the $Cd$

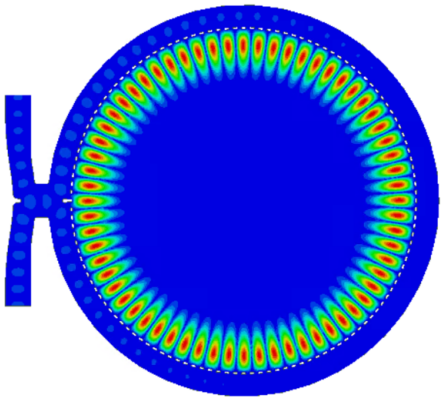

FIG. 9. Field pattern of the BOC storage cavity.

parameter and *Rarc*. The *Cd* parameter is the center of the arc with respect to the center of the cavity, while the *Rarc* is the radius of the arc. The radius of the cavity is the sum of the *Cd* and *Rarc*, which determines the frequency of the cavity and the mode separation.

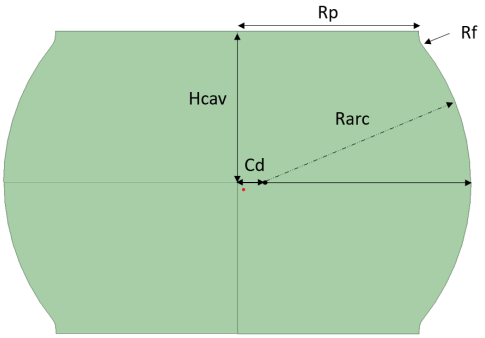


FIG. 10. Shape of the cavity and related parameters.

The smallest RF model to calculate the working mode and nearby modes is shown in the top right corner of Fig. 11. The volume of the RF model is 1/256 of the full cavity and has the copper boundary on the surface of the cavity and electric or magnetic boundaries on the other surfaces of the RF model. The *Cd* parameter was used for the mode separation optimization. The mode separation of the BOC storage cavity is more than 100 MHz. The working frequency is 11.994 GHz and the unloaded quality factor without coupling hole is $2.42 \times 10^5$. The field patterns of the working mode and two nearby modes of $TE_{32,1,4}$ and $TE_{32,1,5}$ with the same azimuthal index are shown in Fig. 11.

To calculate the unloaded factor with coupling hole, a segment RF model was used for this purpose as shown in Fig. 12. The volume of the segment RF model is 1/64 of the full RF model. Several faces are defined for different RF calculations. Face-1 is the surface of the cavity. The Face-2 and Face-3 have the shape described in Fig. 10.

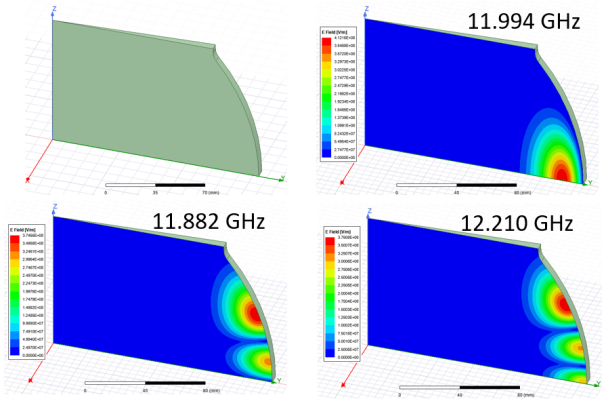


FIG. 11. Smallest RF model as well as the working mode and two nearby modes of $TE_{32,1,4}$ and $TE_{32,1,5}$.

Face-4 is the symmetry plane.

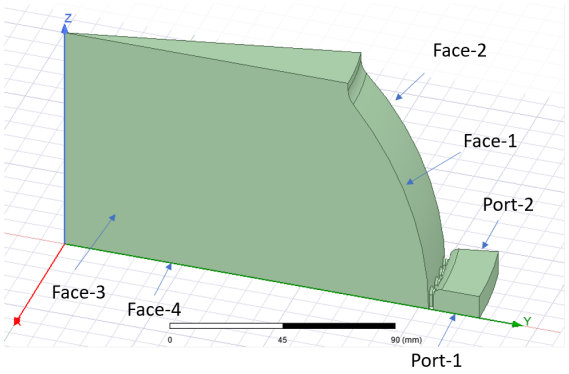


FIG. 12. Segment RF model and definitions of the faces.

Boundary of Face-4 is perfect electric conductor (PEC), while the boundary of face-1 is copper. The Face-2 and Face-3 are primary and slave faces with phase advance of 2 $\pi$. The two ports of the waveguide are used as waveguide ports where the RF power goes in and leave from. The S-parameters of this two-port device is calculated and the result is shown in the Fig. 13. The unloaded quality factor and coupling factor of the segment RF model can be calculated from the s21 of the segment RF model. The method is described in [25]. The unloaded quality factor of the full RF model is same as the segment RF model and the coupling factor of the full RF model is 32 times of the coupling factor of the segment RF model.

The segment RF model is also used to calculate the width of the waveguide around the cavity. In this case, the waveguide part is seen as a resonant cavity results in a different segment RF model with a cavity based on two coupled cells. Both of the two cells should have the same frequency of 11.994 GHz (matching condition). The frequency of the BOC part is 11.994 GHz as mentioned above. The frequency of the waveguide part can be tuned

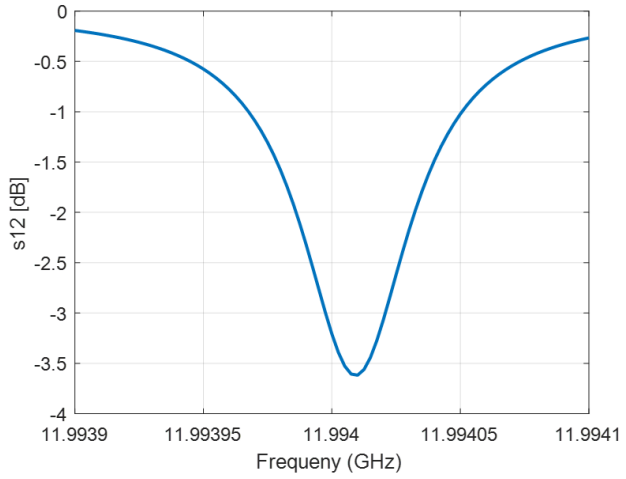


FIG. 13. $S_{12}$ of the segment RF model.

by adjusting the width of the waveguide part. Finally, the frequencies of the 0 mode and the pi mode are $f_0$ and $f_\pi$. The frequency of the waveguide part is calculated by $\sqrt{(f_0^2 + f_\pi^2 - (11.994GHz)^2)}$, which is also 11.994 GHz.

The segment RF model is also used to calculate the surface fields of the BOC storage cavity as shown in Fig. 14. To reduce the surface fields and the RF loss of the waveguide, the height of the waveguide should be as large as possible but still below the cut-off frequency of the next higher order mode. 24 mm is used for the height of the waveguide. The parameters of the surface fields with an input power of 100 MW for the BOC storage cavity are shown in Table IV. The maximum surface magnetic field is the key factor when calculation the pulse heating of the BOC storage cavity. The pulse heating is calculated by using the method in [17] and shown in Fig. 15. The input and output waveforms are needed for the pulse heating calculation. All the parameters of the surface fields are far from their limits which results in an important decision that the RF module with eight accelerating structures need only one BOC storage cavity. For comparison, two BOC storage cavities with a standard height waveguide would be needed for the same RF module.

TABLE IV. Surface fields with an input power of 100 MW for the BOC storage cavity

| Parameters and Units | Values | Limits |
|---|---|---|
| $H_{max}$ [kA/m] | 378.59 | – |
| $E_{max}$ [MV/m] | 14.0 | 100 |
| Sc [MW/mm$^2$] | 0.66 | 2.0 |
| Temperature rise [K] | 48 | 50 |

The cavity has 128 coupling holes. Among the coupling holes, 126 coupling holes have a length of 16 mm and a width of 3.2 mm, as shown in Fig. 16. The minimum thickness of the wall between the cavity and the waveguide is 2 mm.

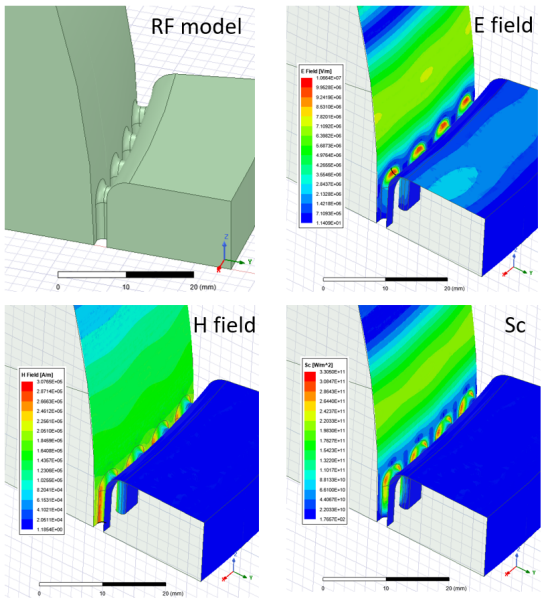


FIG. 14. Surface fields of the BOC storage cavity for an input power of 50 MW.

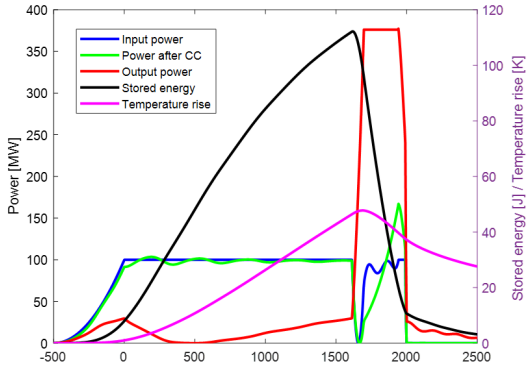


FIG. 15. Pulse heating calculation of the BOC storage cavity for 100 MW input power.

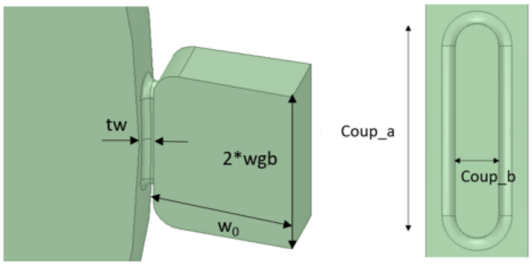


FIG. 16. Parameters of the coupling holes.

A novel RF coupler was designed for BOC. It is a 4-port device as shown in the Fig. 17 The width of the

RF coupler is same as the width of the waveguide of the segment RF model mentioned above. The S-parameters of the RF coupler are shown in Fig. 18. All the RF power going into the Port-1 will leave form Port-2 and the reflection is below -50 dB.

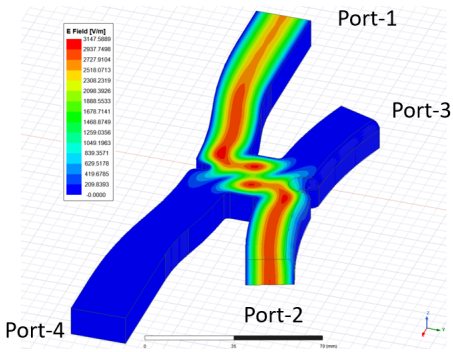


FIG. 17. Core part of the RF coupler.

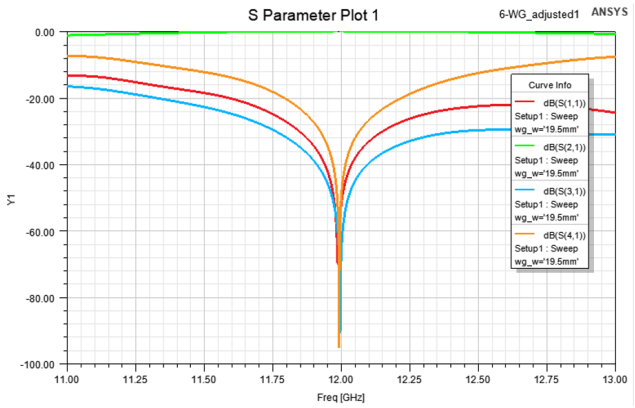


FIG. 18. S-parameters of the core part of the RF coupler.

The full RF coupler with waveguide around the cavity is shown in Fig. 19. The S-parameters of the full RF coupler are shown in Fig. 20. At the working frequency of 11.994 GHz, the reflection is about -46 dB.

The final step for the RF design of the full model of the BOC storage cavity shown in Fig .8 is to reduce the reflection. Two special coupling holes were used, at the entrance and exit of the RF coupler, to reduce the reflection, as shown in Fig. 21. They have different width from that of the normal coupling holes. The width of the two special coupling holes was swept as shown in Fig. 22. The reflection at *coup_b*1 of 4.9 mm is close to the minimum value. It was chosen for the width of the two special coupling holes.

The S-parameters of the Full RF design for the BOC storage cavity are shown in Fig. 23. The maximum reflection around the working frequency of 11.994 GHz is lower than -27 dB and the reflection at the working frequency is -36 dB, which is small enough for the pulse compression system.

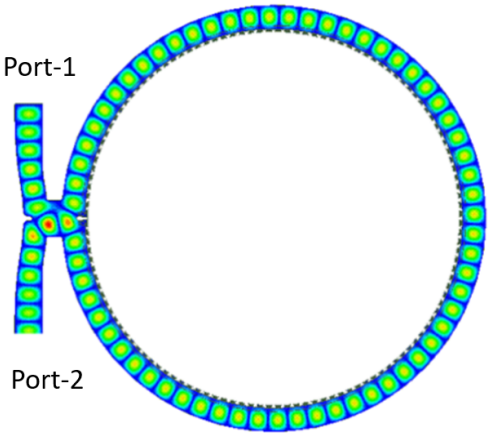


FIG. 19. Full RF model of the RF coupler.

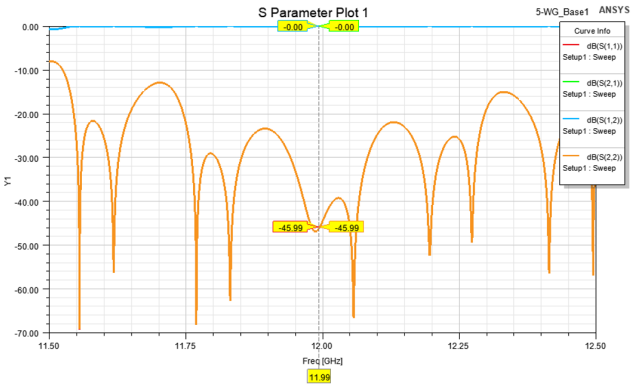


FIG. 20. S-parameters of the full RF coupler.

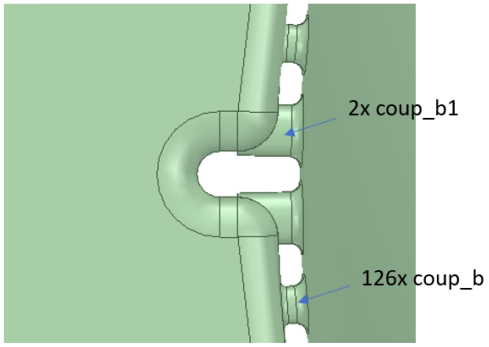


FIG. 21. Two special coupling holes with a width of *coup_b*1.

### B. Mechanical design and thermal analysis

Based on the RF design, the mechanical design of the BOC storage cavity was done. It consists of the following copper parts: the main cavity body with 128 coupling holes, two cooling rings, and an RF coupler, as well as two stainless steel vacuum flanges, as shown in Fig. 24. The top and buttom openings can be used for vacuum

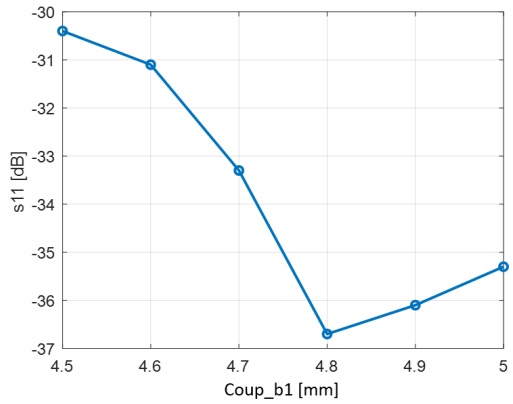


FIG. 22. Reflection of the BOC storage cavity versus the *coup_b*1 .

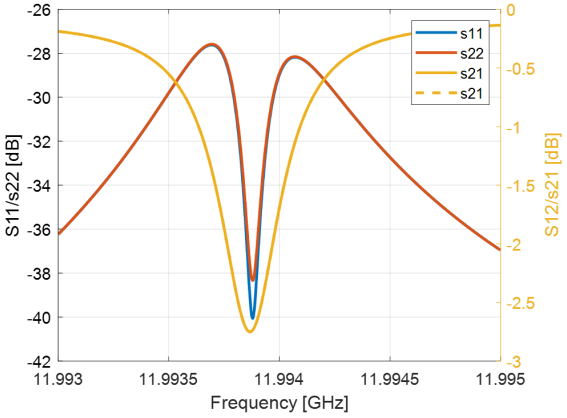


FIG. 23. S-parameters of the BOC storage cavity by using half of the full RF model.

pumping. The body of the main cavity was machined as one part to keep the shape accuracy as high as possible.

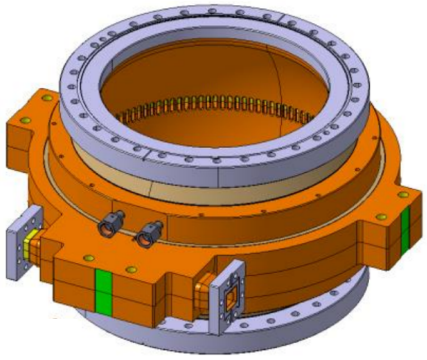

FIG. 24. Mechanical design of the BOC storage cavity.

Based on the mechanical model, the deformations during the final brazing process were calculated as shown in Fig. 25 and Fig. 26. In the y-direction, the maximum deformation is 4.2 um and is located in the coupling holes far from the two special coupling holes. In the z-direction, the maximum deformation is 8.0 um and is located in the waveguide close to the coupling holes with the maximum deformation. Both deformations are less than 0.01 mm, which is negligible for such a large cavity with a diameter of 308 mm.

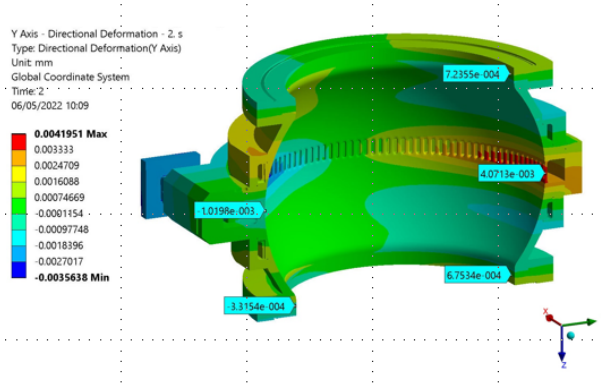


FIG. 25. Deformation calculation of the BOC storage cavity in y direction.

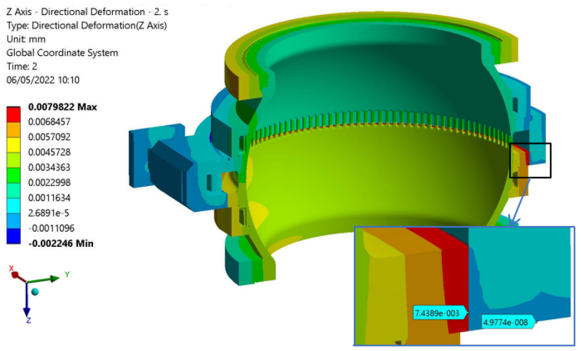


FIG. 26. Deformation calculation of the BOC storage cavity in z direction.

Akin to the RF design, a segment mechanical model which is cut off from the full mechanical model was used for the thermal analysis as shown Fig.27. It consists of three parts: a flange, a cavity, and a cooling ring. The lost RF power in the main cavity is calculated by using the input and output waveforms:

$$P_{\text{loss\_BOC}} = 100[MW] \cdot \frac{\int P_{\text{out\_cc}} dt}{\int P_{\text{in}}\, dt} \cdot \left(1 - \frac{\int P_{\text{out}}\, dt}{\int P_{\text{out\_cc}} dt}\right)$$

, where $P_{\text{in}}$ and $P_{\text{out}}$ are the input and output power of the RF pulse compression system, and $P_{\text{out\_cc}}$ is the output power after the correction cavities. The average power of the main cavity is 2.6 kW with an input RF power of 100 MW, an input pulse length of 2500 ns, and a repetition rate of 50 Hz. The maximum temperature of 39.17 $^0$C (The water temperature for cooling is 22 $^0$C

in the thermal calculation) is at the coupling holes, while the maximum stress intensity of 45.1 MPa is far from the coupling holes. However, the maximum deformation caused by the temperature distribution is far from the coupling holes and is only 22 um, which is also negligible. Based on the mechanical calculations, the mechanical design of the BOC storage cavity is robust and viable.

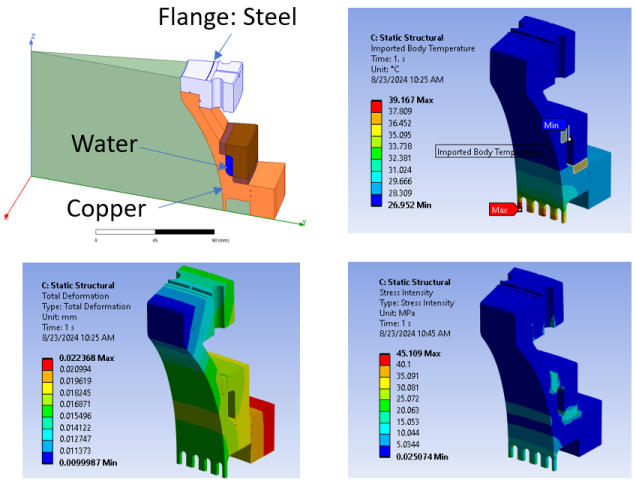


FIG. 27. Theraml calculation of the BOC compressor.

### C. Fabrication of the BOC prototype at CERN

Based on the RF design, the mechanical design, and the mechanical and thermal calculations, the first BOC prototype was fabricated. The fabrication procedure is shown in Fig. 28. The main cavity with 128 coupling holes is the most critical part with the main parameters related to the frequency and coupling factors. Around the main cavity are the RF coupler, the cooling rings, and the steel flanges. The main cavity was roughly machined with a smaller radius. The main cavity was then brazed with the cooling rings and steel flanges prior to the final finish machining. After the brazing, the main cavity was machined with the designed radius of 154.078 mm at a temperature of 20 $^0$C which corresponds to 154.104 mm at the working temperature of 30 $^0$C. The RF coupler was machined and brazed separately before the final brazing. In the final step, the main cavity and the RF coupler were assembled and brazed.

Figure. 29 illustrates the components during the fabrication process. The top-left image shows the main cavity during rough machining. The top-right image features the RF coupler, while the bottom-left image displays the cooling ring. Finally, the bottom-right image depicts the main cavity during the final finishing process.

### D. RF measurement of the BOC prototype

The prototype was measured in four configurations with labels of Full-Open, Open-Front, Full-Close, and Open-Back as shown in Fig. 30. The S-parameters with a span of 5 MHz for the four cases are shown in Fig. 31. RF parameters of the BOC storage cavity were calculated from these S-parameters and shown in Table V. All four cases have the same frequencies that are 1 MHz smaller than the nominal RF design frequency at the nominal operating temperature of 30 $^0$C. In order to correct this fabrication error and maintain operation at nominal Rf frequency of 11.994 GHz, an increase of 5.2 $^0$C in the operating temperature is required. This results in the new operating temperature of 35.2 $^0$C for this first BOC storage cavity prototype.

The unloaded quality factors of the four cases are different from each other which means that some RF power is radiated from the top and bottom of the cavity. This is probably due to fabrication errors in the shape of the cavity. The Full-Closed has the highest unloaded quality which is still smaller than the unloaded qualify of the RF design. Two reasons may cause this reduction in unloaded quality. The first reason is that as some power reach the top and bottom of the cavity closed by the stainless steel flange with larger ohmic loses and small gaps between the cavity and the flanges. The second reason may be that the roughness of the internal surface of the cavity is not good enough. The measured Ra is 0.49 µm. The external quality is 20 % higher than the designed one. This is most probably due to the fabrication error in the wall thickness.

The S-parameters of the Full-Open and Full-Close with a span of 500 MHz are shown in Fig. 32 and Fig. 33. Both of the two cases have the same frequencies of the working mode and nearby modes. The mode separation is larger than 100 MHz from the measurements. It agrees with the RF simulation very well.

Finally, since the frequency of the prototype is acceptable, high-power tests of this first BOC storage cavity prototype are planned at Xbox2 at CERN.

## IV. CORRECTION CAVITY PROTOTYPES: BOWL AND SPHERICAL

In this section, the works of the bowl and spherical correction cavities are presented including the RF design, mechanical design, fabrication and RF measurements. The original bowl correction cavity is based on a E-Rotator[17]. However, in this paper an H-rotator for the correction cavity is presented. In practice, the H-Rotator is easier in fabrication than the E-Rotator.

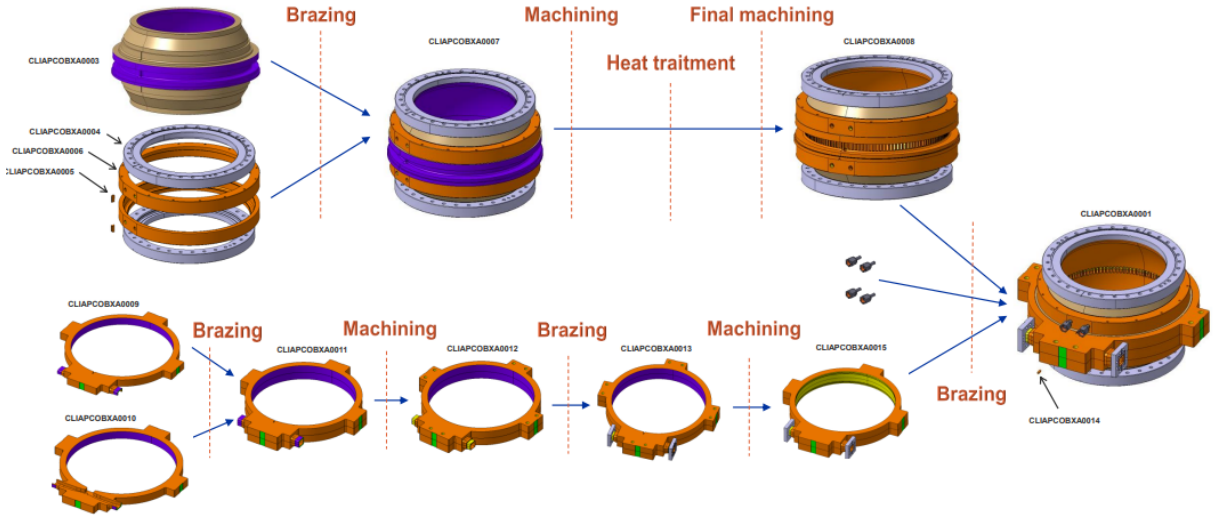


FIG. 28. BOC storage cavity fabrication procedure.

TABLE V. RF parameters of the BOC storage cavity for four cases

| Parameters and Units | RF design | Full-Open | Open-Left | Open-Right | Full-Closed |
|---|---|---|---|---|---|
| Measured Frequency [GHz] | 11.994 | 11.9933 | 11.9933 | 11.9933 | 11.9933 |
| Measured Temperature [$^0$C] | 30.0 | 23.0 | 23.0 | 23.0 | 23.0 |
| Working temp. in vacuum [$^0$C] | 30.0 | 35.2 | 35.2 | 35.2 | 35.2 |
| Unloaded quality | $2.35 \times 10^5$ | $1.89 \times 10^5$ | $1.83 \times 10^5$ | $1.80 \times 10^5$ | $2.06 \times 10^5$ |
| External quality | $3.56 \times 10^4$ | $4.37 \times 10^4$ | $4.27 \times 10^4$ | $4.29 \times 10^4$ | $4.27 \times 10^4$ |
| Coupling factor | 6.6 | 4.3 | 4.3 | 4.3 | 4.8 |

FIG. 29. Components of the BOC prototype under machining.

### A. H-rotator

The H-rotator is used to transfer the RF power from the rectangular input waveguide to the circularly polarized rotating mode of the output circular waveguide. The RF design of the H-rotator is shown in Fig. 34. The original H-Rotator has a height of 10.16 mm, which is the height of the WR90 waveguide and was used for the first correction cavity chain [12].To minimize the surface fields, the height of the H-Rotator was increased from 10.16 to 12 mm. The S-parameters of the optimized H-Rotator are shown in Fig. 35. They are the same as the S-parameters of a standard 3-dB hybrid. The 30 dB passband of the H-Rotator is 80 MHz, which is sufficient for the correction cavities.

Two H-rotator prototypes were fabricated and measured before using them for the correction cavity prototypes as shown in Fig .36 and Fig .37. The results of RF measurements and the corresponding RF simulations are shown in Fig .38. The measured results have good agreements with the simulated ones which makes a conclusion that the two H-rotator prototypes are good enough for the bowl and spherical cavities.

### B. Design of the bowl correction cavity

The new bowl correction cavity was designed taking into account fabrication considerations. The bowl correction cavity consists of a bowl cavity and a H-Rotator as shown in Fig. 39. The S-parameters of the RF de-

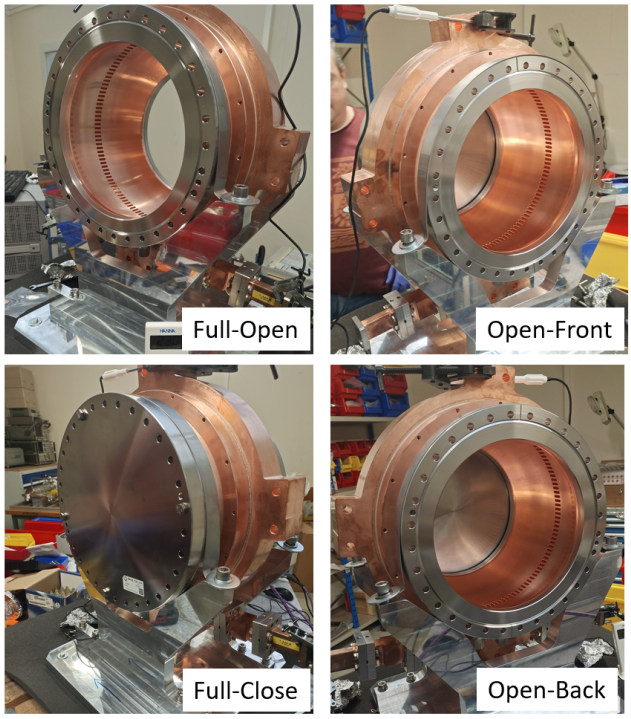


FIG. 30. BOC prototype under RF measurements.

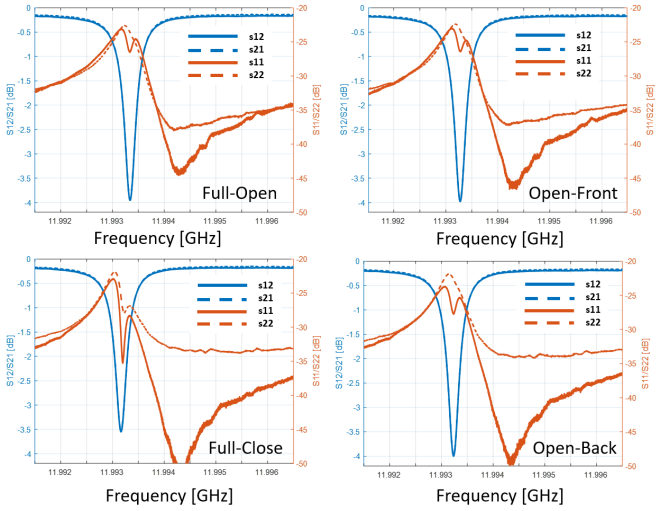


FIG. 31. Measured S-parameters of the BOC storage cavity for four cases.

sign are shown in Fig. 40. The unloaded quality factor is $7.5 \times 10^4$ and the coupling factor is 1.97, which are close to those used in Sec.II. The frequency is 11.9941 GHz which is close to the working frequency of 11.994 GHz, rather than the frequencies of the correction cavities in Table III. The goal of this design is to verify the fabrication process and the high-power performance of this type of cavity. The RF parameters are not necessarily to be the same as those of the final correction cavities. The frequencies of the final correction cavities will be the

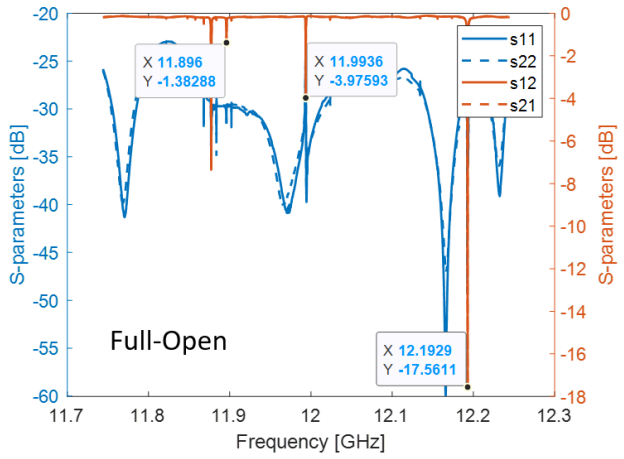


FIG. 32. S-parameters of the BOC with open on one side of the BOC.

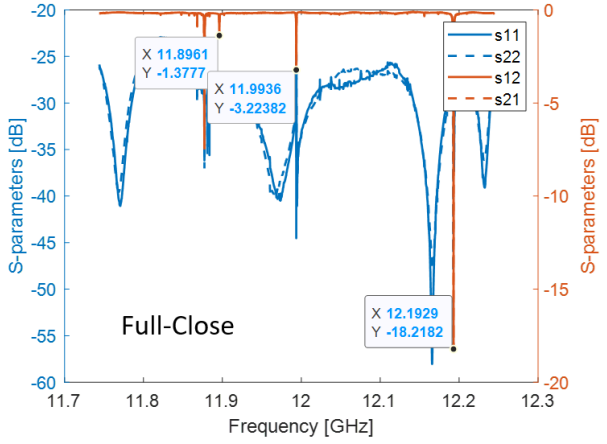


FIG. 33. S-parameters of the BOC with plates on the top and bottom.

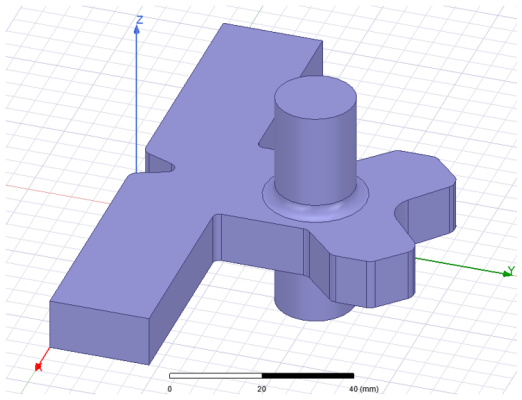


FIG. 34. RF design of the H-Ratotor with a height of 12 mm.

ones in Table III.

Based on the RF design, a mechanical model was designed as shown in Fig. 41. A small straight part is

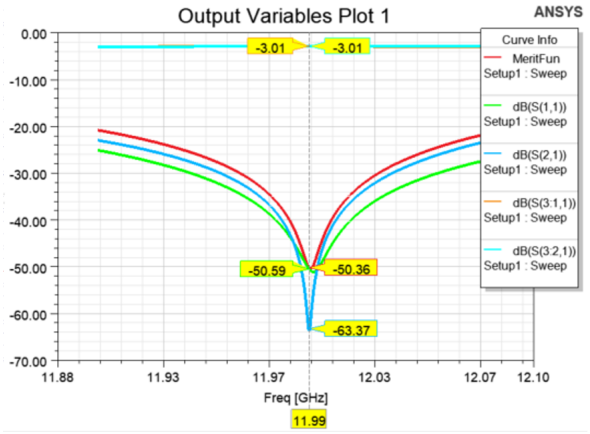


FIG. 35. S-parameters of the H-Rotator with a height of 12 mm.

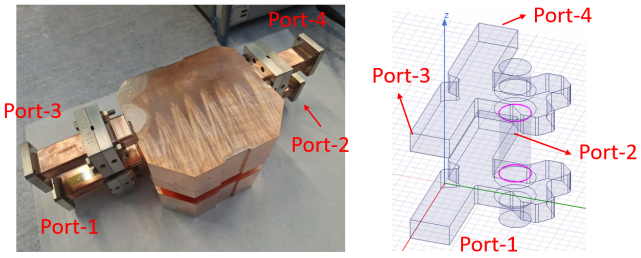


FIG. 36. H-rotator prototypes and the definitions of the ports for the RF measurements.

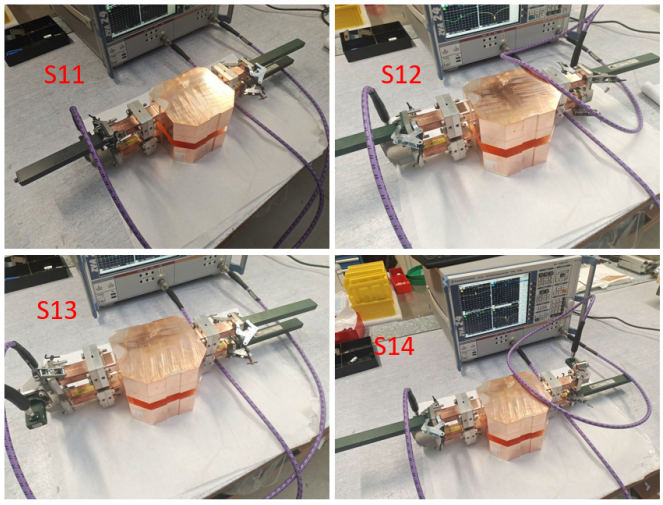


FIG. 37. RF measurements of the H-rotator prototypes.

used for the tuning. Cutting and measuring method was proposed for the tuning procedure. A smaller length of the small straight part is used for the initial fabrication. Then increase the length by machining the bottom face and measure the frequency of the bowl cavity until the frequency is close to the expected frequency.

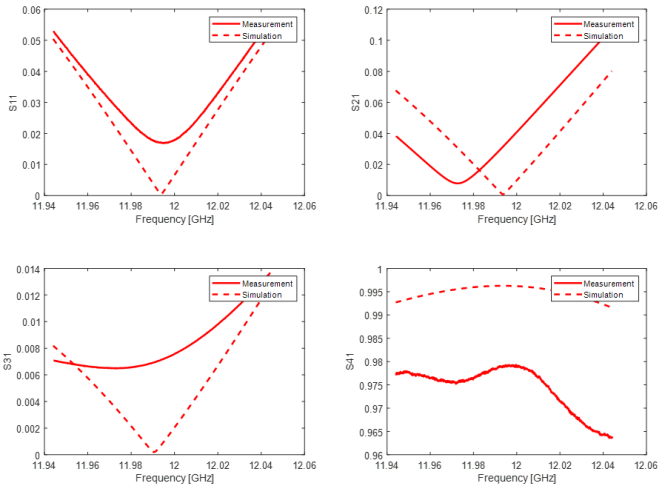


FIG. 38. Measured and simulated results of the H-rotator prototypes.

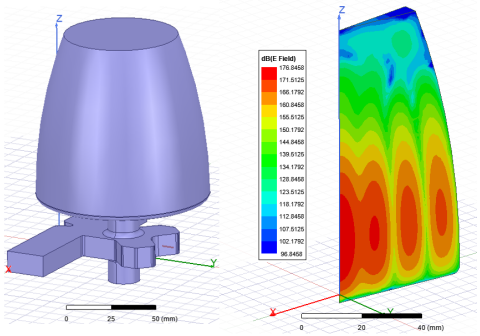

FIG. 39. RF design and field pattern of the bowl correction cavity.

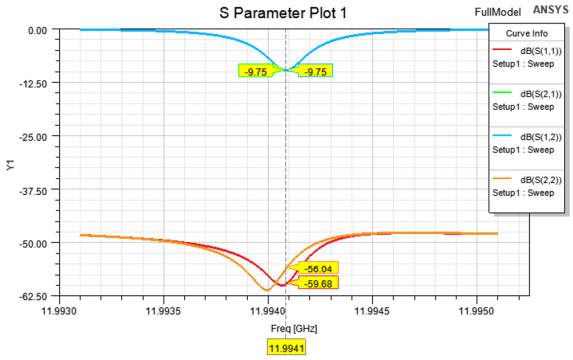


FIG. 40. S-parameters of the Bowl correction cavity.

### C. Measurement of the bowl prototype

A prototype was fabricated as shown in Fig. 42. The bowl correction cavity was measured before and after final brazing, which results in four cases with labels of Closed-BEF, Closed-AFT, Open-BEF, and Open-AFT.

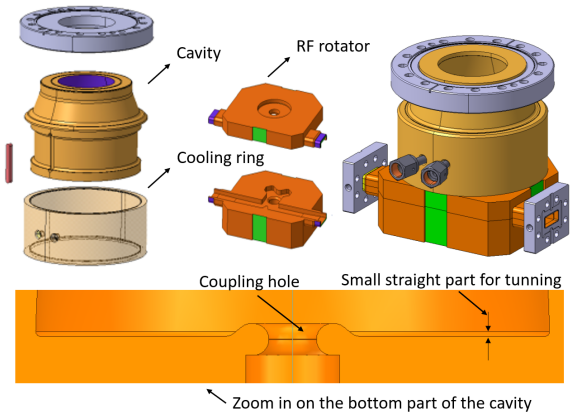


FIG. 41. Mechanical design of the bowl correction cavity.

The measured results are shown in Fig. 43. The RF parameters of the four cases are in Table VI.

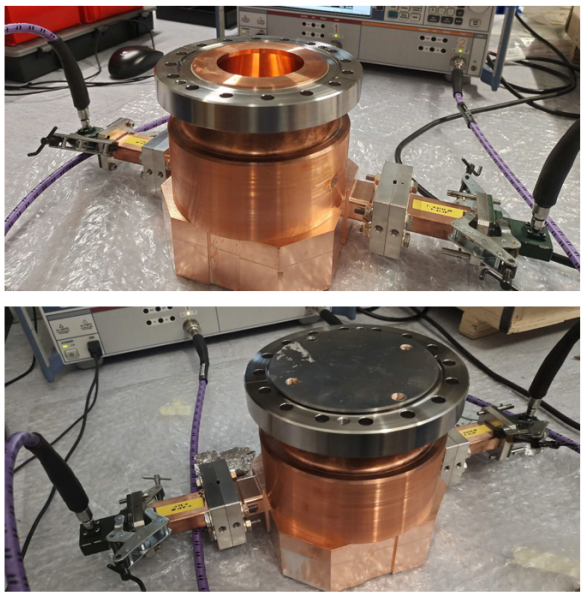

FIG. 42. First prototype of the bowl correction cavity with open top and closed top.

As mentioned above, in principle, there is no field at the top of the bowl cavity. The cover on the top of the bowl cavity should not change any RF parameters of the bowl cavity. However, the unloaded quality factors of the Closed-BEF and Closed-AFT are larger than those of the Open-BEF and Open-AFT, which means that some RF power is radiated from the top of the bowl cavity. The reason of the RF radiation from top of the bowl cavity should be the imperfect shape of the bowl cavity from the fabrication procedure. Another reason for the smaller unloaded quality factor of the bowl prototype is the roughness of the surface. The bowl cavity was machined from the top of the cavity. In this case, the good roughness is difficult to achieve.

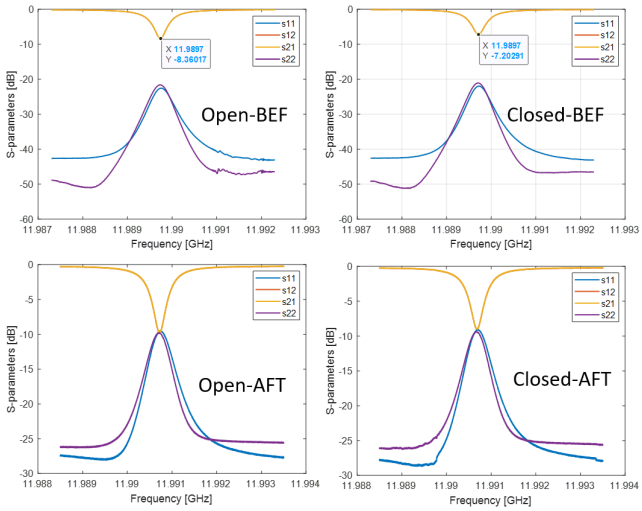


FIG. 43. Measured S-parameters of the bowl correction cavity. Open-BEF: open top before final brazing; Closed-BEF: closed top before final brazing; Open-AFT: open top after final brazing; Closed-AFT: closed top after final brazing

The external quality factors of the bowl prototype are about 30% smaller than that of the RF design. The reason is that a wrong and smaller value was used for the thickness of the coupling hole when the coupling hole was machining.

The working temperatures of the bowl prototype before and final brazing are close to each other. However, they are about 10 $^0$C smaller than that of the RF design. The reason is that a wrong value was used for the small straight part for the tuning on the basis of the cutting and measuring method.

The biggest difference between the measured results before and after the final brazing is the reflections, which are calculated from the $S_{11}$ of the bowl prototype. The reflections are about -22 dB before the final brazing, while they are about -9.6 dB after the final brazing. The reason for the larger reflection is the frequency difference between the eigen frequencies of the two polarizations caused by the shape change of the bowl cavity during the final brazing. The reason for this deformation is not understood. Finally, that is the main reason why this prototype is not suitable for the high-power testing.

### D. Design of the spherical correction cavity

The spherical pulse compressors were widely used in many laboratories, such as SLAC, CERN , KEK, SARI, Tsinghua University, IHEP, Elettra Laboratory and so on[12, 18, 26–30]. The experience and measured results of the existing spherical pulse compressor benefit the design work of the spherical correction cavity. In this section, the work of the spherical correction cavity is presented.

In this paper a spherical cavity with a mode of $TE_{1,1,3}$

TABLE VI. Designed and measured RF parameters of the bowl correction cavity

| Parameters and Units | RF design | Closed-BEF | Closed-AFT | Open-BEF | Open-AFT |
|---|---|---|---|---|---|
| Measured Frequency [GHz] | 11.994 | 11.9897 | 11.9908 | 11.9897 | 11.9908 |
| Measured Temperature [$^0$C] | – | 24.7 | 21.6 | 24.7 | 21.6 |
| Working temp. in vacuum [$^0$C] | 30.0 | 20.0 | 20.8 | 20.0 | 20.8 |
| Unloaded quality factor | $7.5 \times 10^4$ | $6.9 \times 10^4$ | $6.9 \times 10^4$ | $6.1 \times 10^4$ | $6.4 \times 10^4$ |
| External quality factor | $3.81 \times 10^4$ | $2.71 \times 10^4$ | $2.67 \times 10^4$ | $2.74 \times 10^4$ | $2.71 \times 10^4$ |
| Coupling factor | 1.97 | 2.55 | 2.58 | 2.23 | 2.36 |
| Reflection @ Working frequency [dB] | -59.7 | -22.6 | -9.4 | -22.0 | -9.6 |

is designed for the CCs. Based on the H-rotator mentioned above, the spherical correction cavity was designed as shown in Fig. 44. The feature of the cavity is the new coupling hole with a flat part, which compensates for the distortion of the field distribution. The S-parameters of the full RF design are shown in Fig. 45. The reflection of the spherical correction cavity is below -46 dB, which benefits from the central symmetry of the spherical cavity. The unloaded quality factor and the coupling factor were calculated from $S_{12}$. The unloaded quality factor is 7.1e4 and the coupling factor is 1.95.

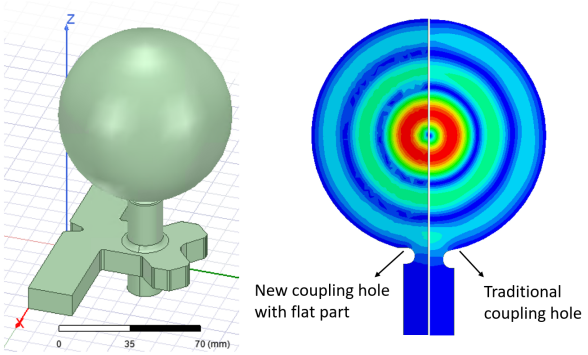


FIG. 44. Full RF design and the $TE_{1,1,3}$ modes of the spherical cavities with different coupling holes.

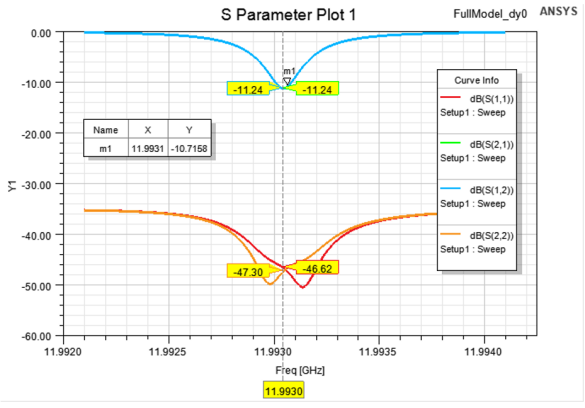


FIG. 45. Designed S-parameters of the spherical correction cavity.

Based on the RF design of the spherical correction cavity, the mechanical model was designed as shown in Fig. 46. The spherical cavity was split into two parts, which facilitates the machining procedure and the surface roughness. Two cooling rings were designed for the up and down half cavities. A tuning feature is designed on the top of the cavity for frequency tuning by means of plastic deformation in case of the frequency error due to fabrication. Mechanical models were calculated to assess the influence of the vacuum pressure on the tuning feature as shown in Fig. 47. The deformation in the region of the hole is 0.23 um, which is negligible.

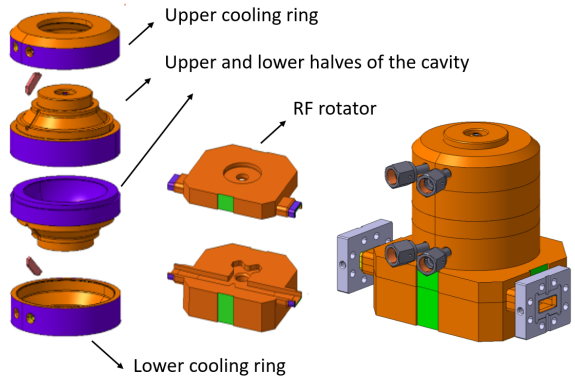


FIG. 46. Mechanical design of the spherical correction cavity.

### E. Measurement of the spherical prototype

A prototype of the spherical correction cavity was fabricated, as shown in Fig. 48. The S-parameters of the spherical correction cavity before and after final brazing were measured. The RF parameters of the RF design and different measurements are calculated based on the measured $S_{12}$ as shown in Tab. VII. The unloaded quality factors and reflections before and after final brazing are close with each other while the frequency difference is about 1 MHz. The designed operating temperature is 30 $^0$C. The calculated from the measurements operating temperatures before and after final brazing are 26.0 $^0$C and 20.5 $^0$C respectively which means that the volume of the spherical cavity was changed slightly during the

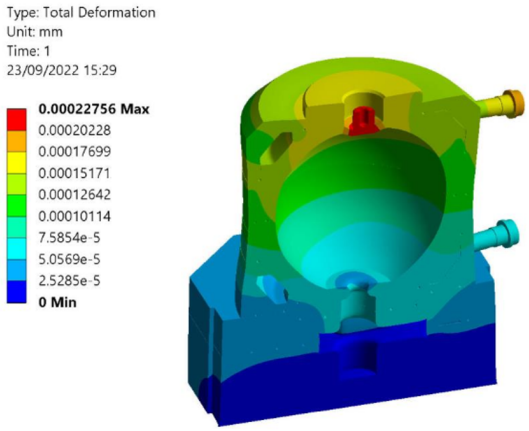


FIG. 47. Deformation of the tuning feature due to vacuum pressure.

brazing procedure. Moreover, the unloaded quality factor and the coupling factor agree very well with those of the RF design.

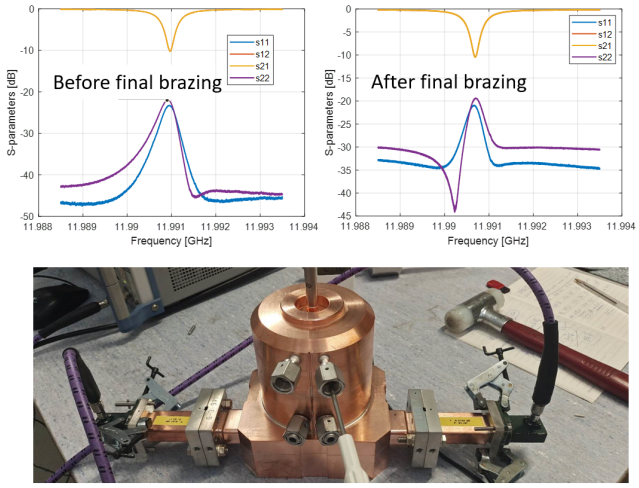


FIG. 48. Prototype of the spherical correction cavity and it's measured S-parameters before and after final brazing.

Since the frequencies of the correction cavities should be specific values, tuning the correction cavity is necessary. The cavity was tuned by using the tuning feature at the top of the cavity. The tuning process is shown in Fig. 49. The final frequency is 11.994 GHz at a nominal operating temperature of 30 $^0$C. After tuning the unloaded quality factor is $6.9 \times 10^4$ and the coupling factor is 2.3. The coupling factor is changed as the tuning change the field pattern which results in the enhancement of field at the coupling hole. Finally, the spherical cavity prototype is suitable for the high-power testing which will be the next step in the prototype validation.

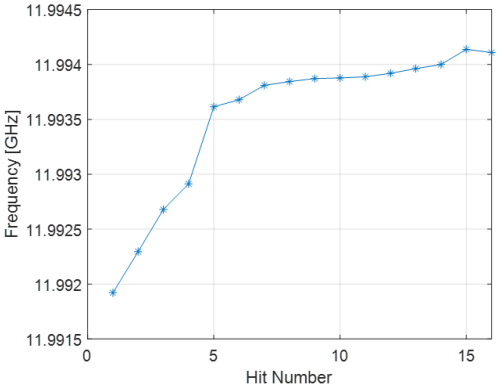


FIG. 49. Tuning process illustrated in terms of the operating frequency at vacuum and 30 $^0$C.

## V. CONCLUSIONS

A new RF pulse compression system was studied for klystron-based CLIC. The shape of the input waveform and the RF loss of the pulse compression system were taken into account for the system design. A new BOC storage cavity works as SC while bowl cavities or spherical cavities work as CCs. Compared with the current pulse compression system at Xbox-2, the power gain is increased by 7 percent and the numbers of the SC and CCs are reduced by a factor of 2. Three prototypes were fabricated and the results are presented and discussed.

For the next step toward the finalization of the pulse compression system, some modifications of the current designs are needed. The roughness of the BOC storage cavity and the bowl correction cavity needs to be improved to achieve a higher unloaded quality factor. A tighter tolerance of the coupling holes of the BOC storage cavity is needed to improve the coupling factor. A smaller Rp of the BOC storage cavity is helpful to eliminate the RF radiation form the top and bottom of the BOC storage cavity. The tuning of the two polarizations of the bowl correction needs to be studied to reduce the reflection.

[1] M. Boland *et al.*, Updated baseline for a staged compact linear collider (2016), arXiv preprint arXiv:1608.07537.
[2] C. L. Collider, last accessed august 12th 2016, URL: http://clic-study. web. cern. ch.
[3] Z. Farkas, H. Hogg, G. Loew, and P. B. Wilson, Sled: A method of doubling slac's energy, in *Proc. Of 9th Int. Conf. On High Energy Accelerators, SLAC* (1974) p. 576.
[4] R. Bossart, P. Brown, J. Mourier, I. V. Syratchev, and L. Tanner, High-power Microwave Pulse Compression of Klystrons by Phase-Modulation of High-Q Storage Cav-

TABLE VII. RF parameters of RF design and measurements before and after final brazing

| Parameters and Units | RF design | Before brazing | After brazing |
|---|---|---|---|
| Frequency @ Air [GHz] | 11.994 | 11.9910 | 11.9907 |
| Measured Temperature [$^0$C] | — | 25.1 | 21.1 |
| Working Temperature [$^0$C] | 30.0 | 26.0 | 20.5 |
| Unloaded Quality Factor | $7.1 \times 10^4$ | $6.9 \times 10^4$ | $6.8 \times 10^4$ |
| Coupling Factor | 1.95 | 1.91 | 1.86 |
| Reflection @ Working frequency [dB] | -48.2 | -23.3 | -21.0 |


ities, (2004).

[5] U. Ellenberger, H. Blumer, M. Heusser, M. Kleeb, L. Paly, M. Probst, T. Stapf, *et al.*, The swissfel c-band rf pulse compressor: Manufacturing and proof of precision by rf measurements, (2014).

[6] C. Wang, W. Fang, Q. Gu, Z. Zhao, and D. Tong, Design and study of a c-band pulse compressor for the sxfel linac, Nuclear Science and Techniques **25** (2014).

[7] C. Kim, S.-J. Park, C.-K. Min, J. Hu, S.-H. Kim, Y. Joo, H. Heo, D.-E. Kim, S. Lee, H.-S. Kang, *et al.*, Review of technical achievements in pal-xfel, AAPPS Bulletin **32**, 15 (2022).

[8] A. Lunin, V. Yakovlev, and A. Grudiev, Analytical solutions for transient and steady state beam loading in arbitrary traveling wave accelerating structures, Phys. Rev. ST Accel. Beams **14**, 052001 (2011).

[9] J. Liu and A. Grudiev, *RF design of accelerating structure for the main linac of the klystron-based first stage of CLIC at 380 GeV*, Tech. Rep. (CERN, Geneva, 2018).

[10] S. Y. Kazakov, Pulse shape correction for rf pulse compression system, Spectrum **5**, 9 (1992).

[11] P. Wilson, Z. Farkas, and R. D. Ruth, *SLED II: A new method of RF pulse compression*, Tech. Rep. (Stanford Linear Accelerator Center, Menlo Park, CA (USA), 1990).

[12] P. Wang, H. Zha, I. Syratchev, J. Shi, and H. Chen, rf design of a pulse compressor with correction cavity chain for klystron-based compact linear collider, Phys. Rev. Accel. Beams **20**, 112001 (2017).

[13] Y. Jiang, H. Zha, P. Wang, J. Shi, H. Chen, W. L. Millar, and I. Syratchev, Demonstration of a cavity-based pulse compression system for pulse shape correction, Phys. Rev. Accel. Beams **22**, 082001 (2019).

[14] X. Lin, H. Zha, J. Shi, Y. Jiang, F. Hu, W. Gu, Q. Gao, and H. Chen, $x$-band two-stage rf pulse compression system with correction cavity chain, Phys. Rev. Accel. Beams **25**, 120401 (2022).

[15] J. Cai and I. Syratchev, *The design update of the X-band RF pulse compressor with Correction Cavities for the CLIC 380 GeV klystron based accelerator*, Tech. Rep. (CERN, Geneva, 2020).

[16] P. Craievich, M. Bopp, H.-H. Braun, A. Citterio, R. Fortunati, R. Ganter, T. Kleeb, F. Marcellini, M. Pedrozzi, E. Prat, S. Reiche, K. Rolli, R. Sieber, A. Grudiev, W. L. Millar, N. Catalan-Lasheras, G. McMonagle, S. Pitman, V. d. P. Romano, K. T. Szypula, W. Wuensch, B. Marchetti, R. Assmann, F. Christie, B. Conrad, R. D'Arcy, M. Foese, P. G. Caminal, M. Hoffmann, M. Huening, R. Jonas, O. Krebs, S. Lederer, D. Marx, J. Osterhoff, M. Reukauff, H. Schlarb, S. Schreiber, G. Tews, M. Vogt, A. d. Z. Wagner, and S. Wesch, Novel $x$-band transverse deflection structure with variable polarization, Phys. Rev. Accel. Beams **23**, 112001 (2020).

[17] X. Wu and A. Grudiev, Novel open cavity design for rotating mode rf pulse compressors, Phys. Rev. Accel. Beams **24**, 112001 (2021).

[18] J. W. Wang, S. G. Tantawi, C. Xu, M. Franzi, P. Krejcik, G. Bowden, S. Condamoor, Y. Ding, V. Dolgashev, J. Eichner, A. Haase, J. R. Lewandowski, and L. Xiao, Development for a supercompact $x$-band pulse compression system and its application at slac, Phys. Rev. Accel. Beams **20**, 110401 (2017).

[19] Y. Jiang, H. Zha, J. Shi, M. Peng, X. Lin, and H. Chen, A compact x-band microwave pulse compressor using a corrugated cylindrical cavity, IEEE Transactions on Microwave Theory and Techniques **69**, 1586 (2021).

[20] P. Wang and A. Grudiev, *Single cylinder cavity based RF cavities for klystron-based Compact Linear Collider*, Tech. Rep. (CERN, Geneva, 2024).

[21] P. Wang, M. Capstick, N. C. Lasheras, S. Doebert, A. Grudiev, C. Rossi, P. M. Sanchez, I. Syratchev, and X. Wu, Design of the rf waveguide network for the klystron-based clic main linac rf module, Nuclear Instruments and Methods in Physics Research Section A: Accelerators, Spectrometers, Detectors and Associated Equipment **1064**, 169410 (2024).

[22] P. Brown and I. Syratchev, 3 ghz barrel open cavity (boc) rf pulse compressor for ctf3, in *2004 IEEE MTT-S International Microwave Symposium Digest (IEEE Cat. No.04CH37535)*, Vol. 2 (2004) pp. 1009–1012 Vol.2.

[23] R. Zennaro, M. Bopp, A. Citterio, R. Reiser, T. Stapf, *et al.*, C-band rf pulse compressor for swissfel, Proc. IPAC , 2827 (2013).

[24] U. Ellenberger, H. Blumer, M. Bopp, A. Citterio, M. Heusser, M. Kleeb, L. Paly, M. Probst, T. Stapf, and R. Zennaro, The swissfel c-band rf pulse compressor: Manufacturing and proof of precision by rf measurements (2014).

[25] P. Wang, J.-R. Shi, Z.-F. Xiong, Z.-N. Liu, C. Cheng, and H.-B. Chen, Novel method to measure unloaded quality factor of resonant cavities at room temperature, Nuclear Science and Techniques **29**, 1 (2018).

[26] T. Higo, H. Ego, Y. Higashi, Y. Bando, A. Saji, K. Ihara, I. Nomura, X. Lin, and J. Shi, Design of s-band spherical-cavity-type pulse compressor for superkekb, (2020).

[27] Z. Li, W. Fang, Q. Gu, and Z. Zhao, Rf design of a c-band compact spherical rf pulse compressor for sxfel, Nuclear Instruments and Methods in Physics Research Section A: Accelerators, Spectrometers, Detectors and Associated Equipment **863**, 7 (2017).

[28] P. Wang, J. Shi, H. Zha, D. Cao, M. Peng, Z. Liu, C. Cheng, and H. Chen, Development of an s-band spher-

ical pulse compressor, Nuclear Instruments and Methods in Physics Research Section A: Accelerators, Spectrometers, Detectors and Associated Equipment **901**, 84 (2018).

[29] J. Lei, X. He, M. Hou, X. Li, G. Pei, H. Wang, J. Zhao, and G. Shu, Rf study and cold test of an s-band spherical cavity pulse compressor, .

[30] N. Shafqat, M. Trovo, I. Cudin, R. Fortunati, F. Gelmetti, L. Giannessi, T. Lucas, F. Marcellini, C. Masciovecchio, M. Milloch, A. Milocco, and R. Zennaro, Fabrication, conditioning and installation of the 1st high gradient s-band accelerating module for the energy upgrade of the fermi free electron laser linac, Nuclear Instruments and Methods in Physics Research Section A: Accelerators, Spectrometers, Detectors and Associated Equipment **1055**, 168543 (2023).